2017

Operational Analysis of Improved Γ-Z-Source Inverter with Clamping Diode and Its Comparative Evaluation

Zeeshan Aleem

Moin Hanif

Operational Analysis of Improved Γ-Z-Source Inverter With Clamping Diode and Its Comparative Evaluation

Zeeshan Aleem, *Student Member, IEEE*, and Moin Hanif, *Member, IEEE*

***Abstract*—Due to a substantial shortage of conventional energy sources, the utilization of renewable energy is gaining attention. Power converters form interfaces to provide power from renewable energy sources to end user systems. Impedance-source inverters (ZSIs) have become a research hotspot and are widely used to overcome the drawbacks of conventional voltage-source inverters and current-source inverters such as two-stage power conversion and less immunity to electromagnetic interference noises. This paper presents various transformer-based ZSIs mainly classified as trans-ZSIs, improved trans-ZSIs, inductor-capacitor-capacitor transformer ZSI, TZSIs, and their comparisons with a new family of ZSIs called Γ-Z-source inverters (ΓZSI). Full operational analysis of an improved ΓZSI with the clamping diode D_2 and its benefits over the conventional ΓZSI are also discussed. The improved ΓZSI utilizes a higher modulation index and consequently a lower duty cycle to achieve same gain, thus reducing the switch voltage stress and providing better output quality. Additionally, an extra diode provides voltage clamping to the dc-link voltage to limit voltage overshoots. The comparative evaluations of all the above mentioned ZSIs are presented in the literature and to validate the advantages of the improved ΓZSI, simulations, and experimental comparisons are also performed.**

***Index Terms*—DC–AC power conversion, high voltage gain, transformers, *Z*-source inverter (ZSI).**

I. Introduction

TRADITIONALLY, there exist two types of power inverters for dc–ac conversion: voltage-source (VSI) and current-source (CSI). Despite their huge demand in industrial applications such as power distribution systems, photovoltaic (PV) systems, and hybrid electric vehicles, they suffer from some severe limitations that make them less preferable. Specifically, for VSIs the obtainable output voltage cannot exceed the input dc voltage, while CSIs output voltage is always higher than the input dc voltage. Therefore, power systems that require both step up/down operations, need an additional dc–dc power converter resulting in a two-stage power conversion with a higher system cost, low efficiency, additional circuitry, and complex control [1]. Moreover, dead time is always required in VSIs to prevent the short circuit but it causes waveform distortion. While, overlap time is the requirement in the CSIs to avoid the open circuit which can destroy the switching devices.

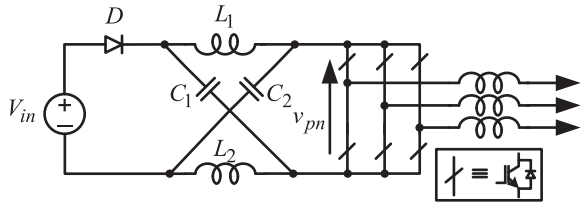

Fig. 1. Classical Z-source inverter.

In order to address these issues, an impedance source inverter (ZSI) was proposed in 2003 [2], as shown in Fig. 1. It creditably utilizes the shorting (shoot-through) of the phase legs to boost the output voltage, and therefore proclaims single-stage power conversion and has a better output waveform quality due to the elimination of dead time. Since the first publication of ZSI, many researchers have focused on developing new *Z*-source topologies with improved modulation schemes, boost capabilities, dynamics, and control methods, and have introduced them in many diversified studies [3]–[32]. In [3], a family of quasi-*Z*-source inverters (qZSIs) were introduced, which have benefits over the ZSIs, such as sharing of common ground, improved input profiles, and lower component voltage stresses. Despite these significant benefits and theoretical infinite voltage gains, all of these qZSIs suffer from one serious drawback, i.e., their practical boost abilities are restricted due to higher component stresses and low output power quality, caused by the tradeoff between the modulation index (M) and the shoot-through duty cycle (D)

$$B = \frac{v_{pn}}{V_{\text{in}}} = \frac{1}{(1-2D)} \tag{1}$$

$$M = 1 - D. \tag{2}$$

The boost factor (B) of the classical qZSI is given in (1), which indicates that for a given input voltage the shoot-through

Manuscript received June 14, 2016; revised October 24, 2016 and January 18, 2017; accepted April 16, 2017. Date of publication May 25, 2017; date of current version October 24, 2017. *(Corresponding Author: Zeeshan Aleem.)*

Z. Aleem is with the Department of Electrical Engineering, University of Cape Town, Cape Town 7701, South Africa (e-mail: zeeshan.aleem18@gmail.com).

M. Hanif is with the Department of Electrical and Electronic Engineering Science, University of Johannesburg, Johannesburg 2006, South Africa, and also with the School of Electrical and Electronic Engineering, Dublin Institute of Technology, Dublin 2, Ireland (e-mail: moinhanif@ieee.org).

Color versions of one or more of the figures in this paper are available online at http://ieeexplore.ieee.org.

Digital Object Identifier 10.1109/TIE.2017.2708358

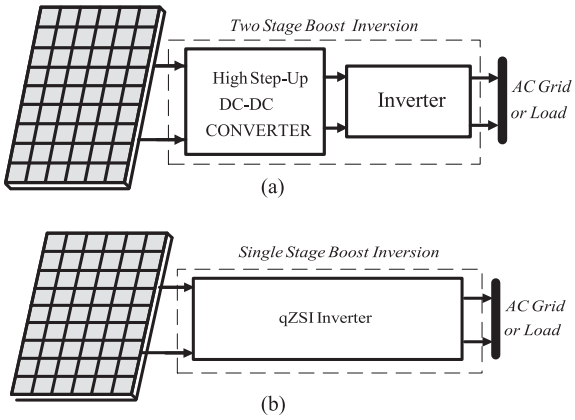

Fig. 2. PV systems. (a) Two-stage power conversion. (b) Single-stage power conversion.

duty cycle can vary from 0 to 0.5 to get the desired output voltage. However, from (2) it can be inferred that for a substantial increase in the shoot-through duty ratio it will consequently utilize a lower modulation index, may be as low as half the maximum value. This will result in poor output waveform quality as the fundamental component of the ac output voltage reduces linearly with modulation index and the total harmonic distortion increases significantly [24]. Moreover, the utilization of higher shoot-through duty ratio leads to higher component voltage stresses and the voltage gain tends to decrease radically.

From the above reasons, the qZSIs are not so much effective in the industrial applications that desire a high step-up inversion of the input voltage. For instance, in PV generation systems, the voltage produced by the solar cells is very low. So one way to increase the input voltage is the serial connection of PV panels, however, it is not recommended because of the substandard power conversion efficiency and reduced lifetime of the PV panels [20]. To overcome this problem, modular systems were proposed as shown in Fig. 2(a), [21]. In these systems, an independent high step converter followed by conventional VSI was applied to the PV panel to increase the output voltage. However, due to the utilization of more switching devices and two-stage power conversion, the cost and complexity of such a system increase. In order to replace these two-stage power conversion systems with single-stage power conversion, (q)ZSIs are utilized as shown in Fig. 2(b). But the boost factor of these (q)ZSIs needs to be enhanced in order to meet the desired output voltage.

Many extensive studies have been performed [4]–[8], [19], [24], [26] to magnify the boosting capability of (q)ZSIs. Several new modulation schemes and circuits are proposed to improve the voltage gains by using a lower shoot-through duty cycle. For example, a family of extended boost ZSIs (diode assisted and capacitor assisted) is proposed in [4], which uses a multiple number of diodes, capacitors, and inductors to enhance the boost factor, which results in the increment of cost and volume of the system. Similarly, in [24], switched inductor (SL) ZSI shown in Fig. 3 is proposed, which replaces the inductors in the impedance network with the SL cells to improve the voltage gain of the inverter. Moreover, to achieve a higher boost factor multiple SL

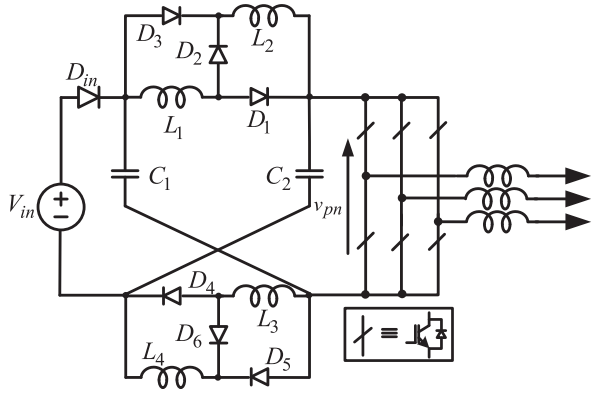

Fig. 3. SL-ZSI.

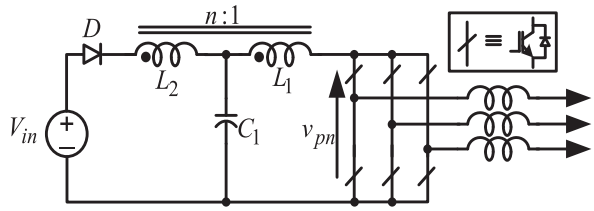

Fig. 4. Trans-Z-source inverter.

cells are used, which result in much higher component count. Despite having higher gains these SL ZSIs suffer from some severe drawbacks, such as discontinuous input current, high component count, absence of common ground between input, and the inverter bridge, and large inrush current at startup.

To overcome these issues, transformer-based ZSIs are proposed [5]–[10] to achieve high voltage gains by keeping the component count as low as possible. These inverters induce a coupled inductor in the *Z*-source network and utilize the turns ratio of the magnetic component to increase the voltage gain of the inverters.

II. Introduction to Transformer-Based ZSI Topologies

This section reviews the different transformer-based ZSI topologies presented in literature.

A. Trans-ZSIs

Fig. 4 shows the basic structure of a trans-*Z*-source inverter [5]. The trans-*Z*-source inverter induces a coupled inductor in the impedance network and the voltage of inductor L_1 is reflected to inductor L_2 through magnetic coupling, therefore capacitor C_2 can be removed from the impedance network. The boost factor B (ratio of dc-link v_{pn} to input voltage) of the trans-*Z*-source inverter is defined as

$$B = \frac{v_{pn}}{V_{\text{in}}} = \frac{1}{(1-(1+n)D)} \tag{3}$$

where n is the turns ratio of the coupled inductor and can be adjusted according to the desired output value. But there are shortcomings associated with trans-ZSIs such as discontinuous input current and huge resonant current at startup.

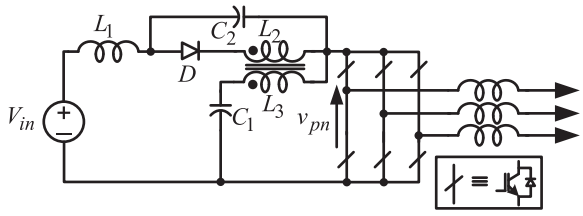

Fig. 5. LCCT-ZSI.

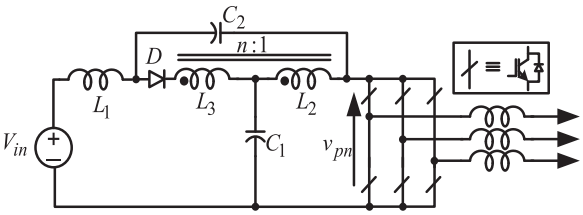

Fig. 6. Improved trans-ZSI.

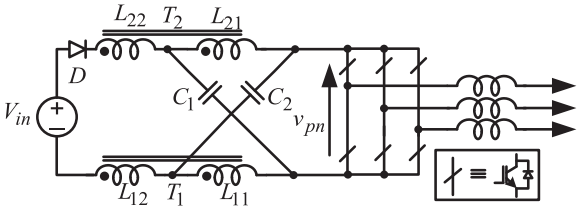

Fig. 7. TZSI.

B. Inductor-Capacitor-Capacitor Transformer (LCCT)-Impedance-source inverter (ZSI)

Fig. 5 shows an LCCT ZSI [6], which adds one additional inductor and capacitor to offer some benefits over the trans-Z-source inverter such as continuous input profiles and reduced inrush current at startup. However, these benefits are attained at the expense of more components while retaining the same voltage gain and other features of trans-ZSI.

C. Improved Trans-ZSI

In [7], improved trans-ZSI was proposed as shown in Fig. 6. The improved trans-ZSI overcomes the issues of trans-ZSI, which are discontinuous input current, inrush current at startup, and unlike LCCT-ZSI, the improved trans-ZSI also provides higher voltage gain compared to LCCT and trans-ZSI. The boost factor is as follows:

$$B = \frac{v_{pn}}{V_{\text{in}}} = \frac{1}{(1-(2+n)D)}. \tag{4}$$

D. TZSIs

Similarly, in 2013 a new family of TZ-source inverters was proposed [8], as shown in Fig. 7. These inverters replace the inductors with the transformers (T_1 and T_2) to achieve a higher gain than conventional trans-Z-source and improved trans-Z-source inverters. The boost ability of the TZSI is expressed as follows:

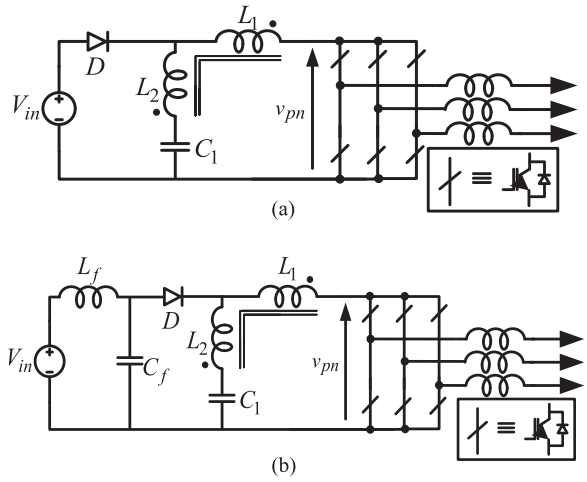

Fig. 8. (a) Conventional ΓZSI. (b) ΓZSI with *LC* filter.

$$B = \frac{v_{pn}}{V_{\text{in}}} = \frac{1}{(1-(2+n_1+n_2)D)} \tag{5}$$

where n_1 is the turns ratio of T_1 and n_1 is the turns ratio of T_2. The voltage gain of the inverter is adjusted by varying the turns ratio of the transformers. Even with a turns ratio of 1 ($n_1 = n_2 = 1$) the TZSIs produces higher gain than the trans-ZSIs. However, there are disadvantages associated with TZSIs such as absence of common ground between the input and inverter bridge, utilization of two transformers results in increased size and cost of the system and discontinuous input current.

Although the inverters discussed earlier are attractive and have several significant features, the transformer turns ratio might become too high for obtaining high voltage gain, which leads to oversized and bulky transformers. They also require isolation between the windings that cause the leakage inductance to create voltage spikes. Siwakoti *et al.* [9], Loh *et al.* [10], and Banaei *et al.* [11] propose a new type of ZSIs called Γ-Z-source inverter (ΓZSI) that uses the opposite approach to boost the output voltage discussed in the next section.

III. ΓZSI and Improved ΓZSI With Clamping Diode

The ΓZSI, shown in Fig. 8(a), boosts the output voltage by lowering the turns ratio of the transformer rather than increasing it. As compared to other transformer based impedance source topologies, the ΓZSI uses the same or less number of components for producing higher voltage gain while utilizing a higher modulation index and consequently a lower shoot-through duty ratio. Moreover, the output voltage of the ΓZSI is adjusted by varying the turns ratio of the magnetic component within a narrow range of $1<n\leq 2$. This leads to lesser winding turns and confined transformer size to achieve higher gain, which makes it more preferable in the industrial applications. The boost ability of the ΓZSI is expressed as

$$B = \frac{v_{pn}}{V_{\text{in}}} = \frac{1}{(1-(1+1/n-1)\,D)}. \tag{6}$$

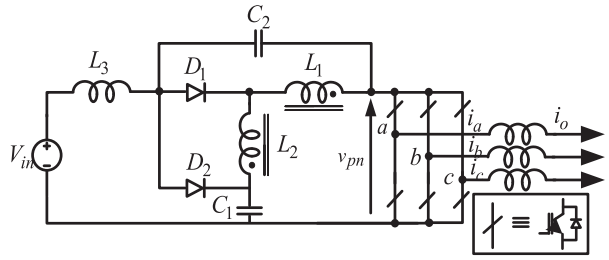

Fig. 9. Improved ΓZSI with clamping diode.

However, despite having these benefits, the ΓZSI suffers from several serious drawbacks.

1) The input current is discontinuous, thus requiring an additional *LC* filter at the front end of the ΓZSI as shown in Fig. 8(b) [11], to eliminate the discontinuity of the input current and protect the energy source.
2) There is huge inrush current at startup and the resulting voltage and current spikes can damage the devices. It appears due to large resonant current flowing in to the input diode, transformer windings, capacitor, and body diodes of the insulated gate bipolar transistors (IGBTs).
3) The ΓZSI uses the same number of components as of trans-ZSI, but with a different transformer placement. This difference in dot polarities of the magnetic component causes the capacitor C1 current to bypass, which is very high. This leads in the increment of current ratings and cost of the switching devices.
4) The leakage inductance of the transformer is utilized to minimize the current of capacitor C1, however the leakage inductance is in series with the inverter bridge without any snubber circuit causing large voltage spikes due to the switching of the winding currents.

This paper presents and analyzes the improved ΓZSI that enhances upon the conventional ΓZSI to overcome the aforementioned drawbacks. Fig. 9 shows the basic structure of the improved ΓZSI, which can be derived by rearranging the components of Fig. 8(b) and by adding a clamping diode D_2.

The main features of the improved ΓZSI are as follows.

1) The input current is continuous and no additional filter is required.
2) It provides startup inrush current suppression, unlike the trans-ZSI, tZSI, and ΓZSI, because no current flows into the main circuit at startup.
3) In other transformer-based *Z*-source topologies, the energy stored in the leakage inductance of the transformer produces voltage spikes across the inverter bridge, while in the improved ΓZSI inverter, the clamping diode forms a new high-frequency loop comprising of $C_2 - D_2 - C_1$. As a result, the dc-link voltage is clamped to $(V_{c1} + V_{c2})$, thus eliminating the voltage spikes across the inverter bridge.
4) The improved ΓZSI with clamping diode has higher voltage gain than the original ΓZSI and above discussed topologies such that with same input/output conditions and same transformer turns ratio, the improved ΓZSI uses a lower shoot through duty cycle and consequently a higher modulation index as compared to original ΓZSI, which results in lower component voltage stress and better output power quality.

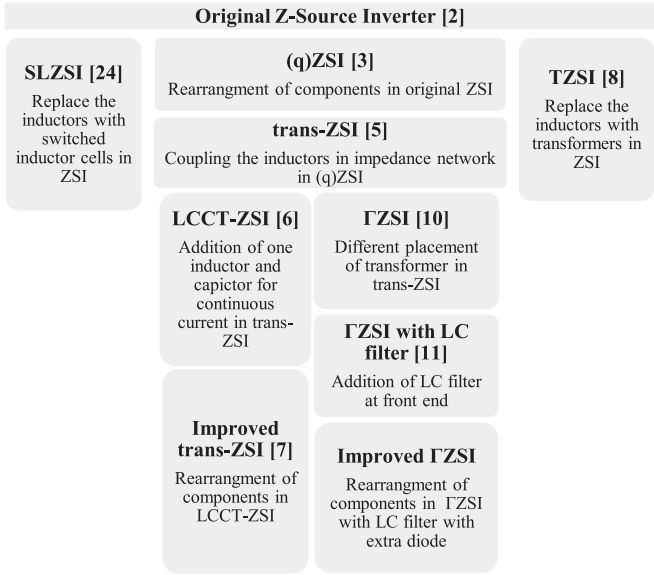

Fig. 10. Flowchart diagram of derivation of improved ΓZSI from the original ZSI.

Fig. 10 shows a flowchart diagram of derivation of improved ΓZSI with clamping diode from the original ZSI.

A. Operating Principle of the Improved ΓZSI With Clamping Diode

Like all the other existing ZSIs, the improved ΓZSI inverter with clamping diode have one extra shoot-through state besides the two traditional zero states and six active states. For analytical purposes, the operating states are simplified as shoot-through state and nonshoot-through state. The equivalent circuits of the improved ΓZSI inverter during these operating states are shown in Fig. 11(a) and (b).

Mode 1: In the shoot-through state, all the switches of the same legs are turned ON and the circuit is equivalent to a short circuit. During this shoot-through state both the diodes are "OFF" and the windings 1 and 2 are charged by the capacitor current C_1.

Mode 2: The nonshoot-through state consists of two zero states and six active states, in this mode both the diodes are "ON" and stored energy in the windings are released to the circuit and the load, thus the capacitors C_1 and C_2 are charged by it. During this state, the energy stored in the leakage inductances is absorbed by C_1 and C_2 through diode D_2 and it is, therefore, recycled without creating voltage spikes.

B. Boost Ability of the Improved ΓZSI With Clamping Diode

The boost factor of the inverter is the ratio of dc-link voltage of the inverter bridge v_{pn} to the input dc voltage. Fig. 11(a) and (b) shows the simplified equivalent circuits of the improved ΓZSI inverter with clamping diode during the shoot-through and non-shoot-through states.

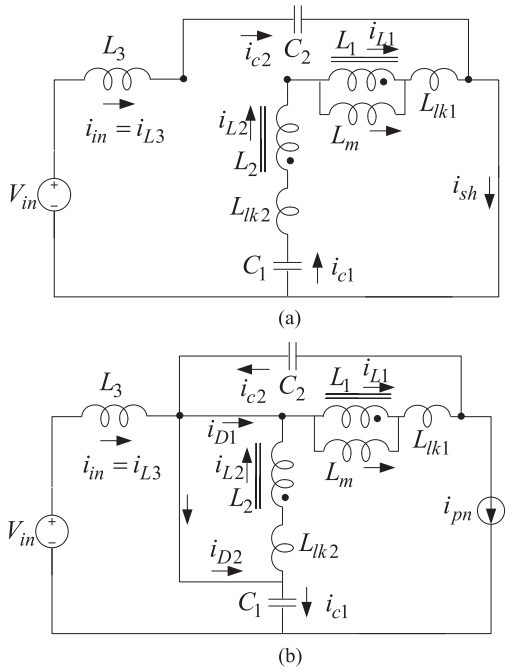

Fig. 11. Operation modes of the improved ΓZSI with clamping diode. (a) Mode 1: Shoot-through state. (b) Mode 2: Active state (nonshoot-through state).

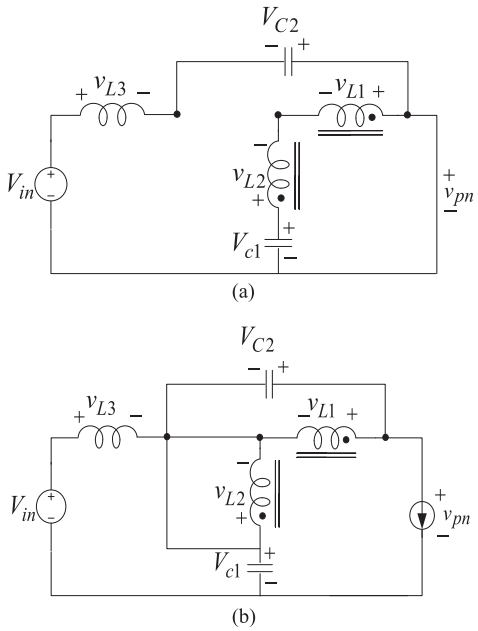

Fig. 12. Simplified circuits. (a) Shoot-through state. (b) Nonshoot-through state.

By applying Kirchhoff's Voltage Law (KVL) to the circuit in Fig. 12(a) in shoot through state, we obtain

$$\begin{cases} -V_{c1} + v_{L2\_sh} - v_{L1\_sh} = 0 \\ v_{L1\_sh} = v_{L2\_sh} - V_{c1} - - - -(\text{i}) \\ n = \dfrac{v_{L1}}{v_{L2}} \\ -V_{\text{in}} + v_{L3\_sh} - V_{c2} = 0 \\ v_{L3\_sh} = V_{\text{in}} + V_{c2} - - - -(\text{ii}). \end{cases} \tag{7}$$

Similarly, by applying KVL to the circuit in Fig. 12(b), we obtain

$$\begin{cases} -V_{c1} - v_{L2\_non} + v_{L1\_non} + v_{pn} = 0 \\ -V_{\text{in}} - v_{L3\_non} + v_{L2\_non} + V_{c1} = 0 \\ v_{L3\_non} = -V_{\text{in}} + v_{L2\_non} + V_{c1} \\ v_{L3\_non} = v_{pn} - V_{in} - V_{c2} - - - -(\text{iii}) \\ v_{L1\_non} = -V_{c2} \\ n v_{L2\_non} = -V_{c2}. \end{cases} \tag{8}$$

By applying the flux balance condition across L_1 and L_2, we have

$$\begin{cases} v_{L2\_sh} D = v_{L2\_non}(1-D) \\ v_{L2\_sh} = -V_{c2}\dfrac{(1-D)}{nD} \\ v_{L1\_sh} D = v_{L1\_non}(1-D) \\ v_{L1\_sh} = -V_{c2}\dfrac{(1-D)}{D} - - - -(\text{iv}). \end{cases} \tag{9}$$

By substituting (iv) in (i), we have

$$\begin{cases} v_{L1\_sh} = v_{L2\_sh} - V_{c1} \\ -V_{c2}\dfrac{(1-D)}{D} = -V_{c2}\dfrac{(1-D)}{nD} - V_{c1} \\ V_{c1} = V_{c2}\dfrac{(1-D)(n-1)}{nD} - - - -(\text{v}). \end{cases} \tag{10}$$

By applying voltage second condition across L_3, yields

$$\begin{cases} (V_{\text{in}} + V_{c2})\, D = (v_{L2\_non} - V_{\text{in}} + V_{c1})\,(1-D) \\ V_{c2} = \dfrac{V_{\text{in}}(nD)}{n(1-2D) - 1 + D} - - - (\text{vi}). \end{cases} \tag{11}$$

By substituting (vi) in (v), we have

$$V_{c1} = \frac{V_{\text{in}}(1-D)(n-1)}{n(1-2D) - 1 + D} \tag{12}$$

where n is the turns ratio of the transformer, V_{in} is the input voltage, and DD is the shoot through duty of the improved ΓZSI with clamping diode.

By (ii) and (iii), we can find the dc-link voltage, v_{pn} of the improved ΓZSI with clamping diode, which is expressed as

$$\begin{cases} (V_{\text{in}} + V_{c2})\, D = (v_{pn} - V_{\text{in}} - V_{c2})\,(1-D) \\ v_{pn} = \dfrac{V_{\text{in}}(n-1)}{(n(1-2D) - 1 + D)}. \end{cases} \tag{13}$$

Therefore, the boost factor B of the improved ΓZSI with clamping diode is given by

$$B = \frac{(n-1)}{(n(1-2D) - 1 + D)}. \tag{14}$$

IV. Comparative Evaluations

To validate the benefits of the improved ΓZSI with clamping diode, comparisons with the previously proposed topologies have been made in this section. The plot of boost factor B versus duty cycle D for the improved ΓZSI, TZSI, ΓZSI, trans-ZSI, and improved trans-ZSI has been shown in Fig. 13. The turns

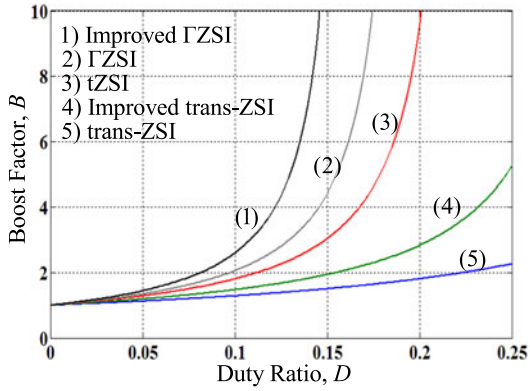

Fig. 13. Plot of boost factor versus duty cycle with $n = 1.24$.

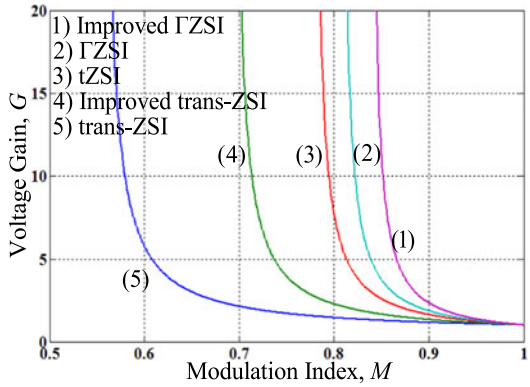

Fig. 14. Voltage gain against modulation index plot with $n = 1.24$.

ratio of the transformers has been set to 1.24 for each of inverter topologies for the sake of comparisons. From the plot, it can be inferred that the boosting capacity of the improved ΓZSI with clamping diode is significantly greater than that of other topologies with same number of turns.

All of the pulse width modulation schemes, developed for the ZSIs, which are simple boost control, maximum boost control, and constant boost control [11]–[13] are applicable to the improved ΓZSI with clamping diode as well. The simple boost control scheme has been applied in this study. The relation between the modulation index and the duty ratio in simple boost scheme is expressed as

$$M = 1 - D. \tag{15}$$

The output phase peak voltage v_{ph} of the ZSIs is defined as

$$\hat{v_{ph}} = \frac{\mathrm{MBV_{in}}}{2}. \tag{16}$$

Therefore, from (15) and (16), the voltage gain G can be expressed in terms of modulation index as

$$G(\mathrm{MB}) = \frac{\hat{v_{ph}}}{V_{\mathrm{in}}/2} = \frac{M(n-1)}{M(2n-1)-n}. \tag{17}$$

Fig. 14 shows the voltage gain versus modulation index graph for the improved ΓZSI, tZSI, ΓZSI, trans-ZSI, and improved trans-ZSI. From Fig. 14, it can be observed that with the decrement in modulation index the voltage gain rises. Thus, for

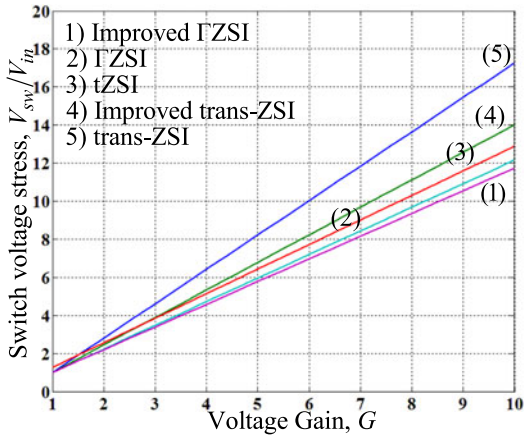

Fig. 15. Plot of voltage stress versus voltage gain with $n = 1.24$.

the same voltage gain compared with other impedance source topologies the improved ΓZSI utilizes higher modulation index and consequently a lower shoot-through duty ratio, which results in lower stress across the inverter bridge, better output quality, and overall better spectral performance.

Another main concern associated with the ZSIs is the voltage stress across the switching devices. The voltage stress across the inverter bridge is the same as the dc-link voltage for every ZSI which is expressed as:

$$V_{sw} = v_{pn} = BV_{\mathrm{in}}. \tag{18}$$

By using the relation in (18) and (14), the voltage stress of the improved ΓZSI with clamping diode in terms of voltage gain can be obtained as

$$\frac{V_{sw}}{V_{\mathrm{in}}} = \frac{G(2n-1)+1-n}{n}. \tag{19}$$

The plot of switch voltage stress versus the voltage gain is shown in Fig. 15. As discussed earlier, for obtaining the same voltage gain the improved ΓZSI with clamping diode utilizes a higher modulation index with lower shoot through duty cycle resulting in lower voltage stresses across the switching devices. Thus, it is clearly shown in the Fig. 15 that for the same gain, the voltage stress of the improved ΓZSI is the lowest among the other mentioned impedance source topologies. This makes improved ΓZSI with clamping diode a good practical candidate for the industrial applications that requires higher boost abilities with cost efficient demands.

Table I compares the governing equations for improved ΓZSI with clamping diode, ΓZSI, TZSI, trans-ZSI, and improved trans-ZSI. It summarizes all the voltage stresses under the conditions of same input voltage and same shoot-through duty cycle. In Table I, S_D represents the shoot-through switching function, which is defined as "1" when the inverters are in shoot-through states and as "0" when the inverters are in nonshoot-through states. In Table I, v_{pn} is dc-link voltage of the inverter, V_c is the voltage across the capacitor, V_D is the voltage of the input diode, D is the shoot-through duty cycle, and n is the turns ratio of the transformer.

TABLE I

	Trans-ZSI, Fig. 4	Improved trans-ZSI, Fig. 6	TZSI, Fig. 7	ΓZSI, Fig. 8(a), (b)	Improved ΓZSI With Clamping Diode, Fig. 9
v_{pn} (V_{sw})	$\overline{S_D} \cdot \left(\frac{V_{\rm in}}{1-(1+n)D}\right)$	$\overline{S_D} \cdot \left(\frac{V_{\rm in}}{1-(2+n)D}\right)$	$\overline{S_D} \cdot \left(\frac{V_{\rm in}}{1-(2+n_1+n_2)D}\right)$	$\overline{S_D} \cdot \left(\frac{V_{\rm in}}{1-(1+1/n-1)D}\right)$	$\overline{S_D} \cdot \left(\frac{(n-1)(V_{\rm in})}{(n(1-2D)-1+D)}\right)$
V_c	$V_{c1} = \frac{(1-D)(V_{\rm in})}{1-(1+n)D}$ $V_{c2} = NA$	$V_{c1} = \frac{(1-D)(V_{\rm in})}{1-(2+n)D}$ $V_{c2} = \frac{(1+n)(V_{\rm in})}{1-(2+n)D}$	$V_c = \frac{(1+n_1+n_2)(D)(V_{\rm in})}{1-(2+n_1+n_2)D}$ $V_c = V_{c1} = V_{c2}$	$V_{c1} = \frac{(1-D)(V_{\rm in})}{1-(1+1/n-1)D}$ $V_{c2} = NA$	$V_{c1} = \frac{V_{\rm in}(1-D)(n-1)}{n(1-2D)-1+D}$ $V_{c2} = \frac{V_{\rm in}(nD)}{n(1-2D)-1+D}$
V_D	$S_D \cdot \left(\frac{nV_{\rm in}}{1-(1+n)D}\right)$	$S_D \cdot \left(\frac{(1-n)V_{\rm in}}{1-(2+n)D}\right)$	$S_D \cdot \left(\frac{(1+n_1+n_2)V_{\rm in}}{1-(2+n_1+n_2)D}\right)$	$S_D \cdot \left(\frac{V_{\rm in}}{n-1-nD}\right)$	$V_{D1} = S_D \cdot \left(\frac{nV_{\rm in}}{(n(1-2D)-1+D)}\right)$ $V_{D2} = S_D \cdot \left(\frac{(n-1+D)V_{\rm in}}{(n(1-2D)-1+D)}\right)$
$G = \text{MB}$	$\frac{M}{1-(1+n)(1-M)}$	$\frac{M}{1-(2+n)(1-M)}$	$\frac{M}{1-(2+n_1+n_2)(1-M)}$	$\frac{M}{1-(1+1/n-1)(1-M)}$	$\frac{(n-1)(M)}{(n(2M-1)-M)}$

V. Simulation and Experimental Results

Saber simulations and experiments are performed to validate the operation of the improved ΓZSI with clamping diode. In simulations, all parameters are considered ideal. Simulations are performed for both converters to validate the advantages of the improved ΓZSI with clamping diode over the conventional ΓZSI. Simple boost modulation scheme is applied. Below are the detailed electrical specifications:

1) input voltage: $V_{\rm in} = 152$ V;
2) output voltage: 220 $V_{\rm rms}$;
3) coupled inductor: $L_1 = 200$ μH, $L_2 = 130$ μH;
4) inductor: $L_3 = 500$ μH;
5) Z-source capacitors: $C_1 = C_2 = 100$ μF;
6) modulation index: $M = 0.9$;
7) switching frequency: $f_{sw} = 20$ kHz;
8) output ac filter inductors: $L_o = 850$ μH;
9) output ac filter capacitors: $C_o = 100$ μF;
10) resistive load: $R = 20$ Ω/phase.

For the sake of comparisons and explaining the issues faced with conventional ΓZSI, simulations are presented for both conventional ΓZSI and improved ΓZSI with clamping diode. Fig. 16 shows the waveforms of the conventional ΓZSI with shoot through duty 0.1 and modulation index 0.9, the dc-link voltage is boosted to 314 V. Fig. 16(a) shows the waveforms of dc-link voltage with $L_{\rm lkp} = L_{\rm lks} =$ 300 nH and shoot-through current. Fig. 16(b) shows the large inrush current at startup and the expanded waveforms of discontinuous input current.

Fig. 17 shows the simulation results of improved ΓZSI with clamping diode. Fig. 17(a) shows the waveforms of the improved ΓZSI inverter dc-link voltage and shoot through current. From the results, it can be realized that the voltage spikes caused by the leakage inductances are minimized with the addition of the extra diode. Additionally, with the same electrical parameters the dc-link voltage of the improved ΓZSI with clamping diode is boosted to 400 V, which is higher than the original ΓZSI. Fig. 17(b) shows the suppressed inrush current and expanded input current waveform. As it can be seen from the waveform, the input current is continuous, thus no additional filter is required at the front end. Fig. 17(c) shows the waveforms of line-to-line output voltage, output current and input voltage.

A hardware prototype of improved ΓZSI with clamping diode is fabricated and experiments are performed to validate its

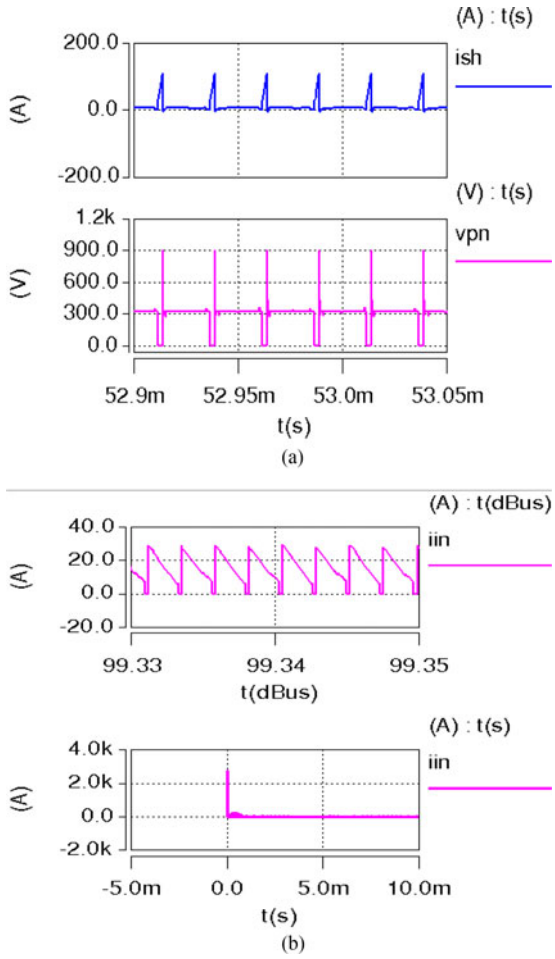

Fig. 16. Simulation results of the conventional Γ-ZSI.

advantages. Simple boost control signals are generated using a DSP-kit based on TMS320f28335. All the parameters in experiments are kept same as in simulations. Fig. 18(a) shows the experimental waveforms of input voltage $V_{\rm in}$, line-to-line output voltage v_{ab}, and output current i_a. Fig. 18(b) shows the waveforms across the Z-source network capacitors C_1 and C_2, and comply with the derived theoretical (11) and (12). Fig. 19(a) and (b) shows the waveforms of input current and dc-link voltage v_{pn} of the improved ΓZSI, i.e., with D_2 in Fig. 19(a) and

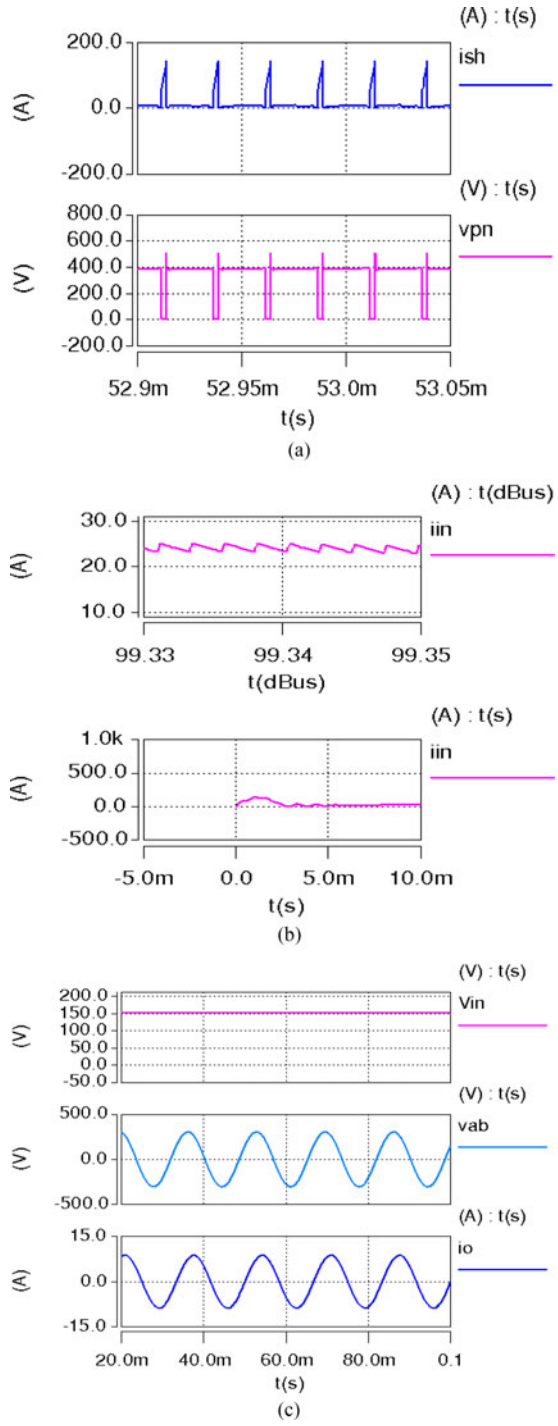

Fig. 17. Simulation results of improved Γ-ZSI with clamping diode.

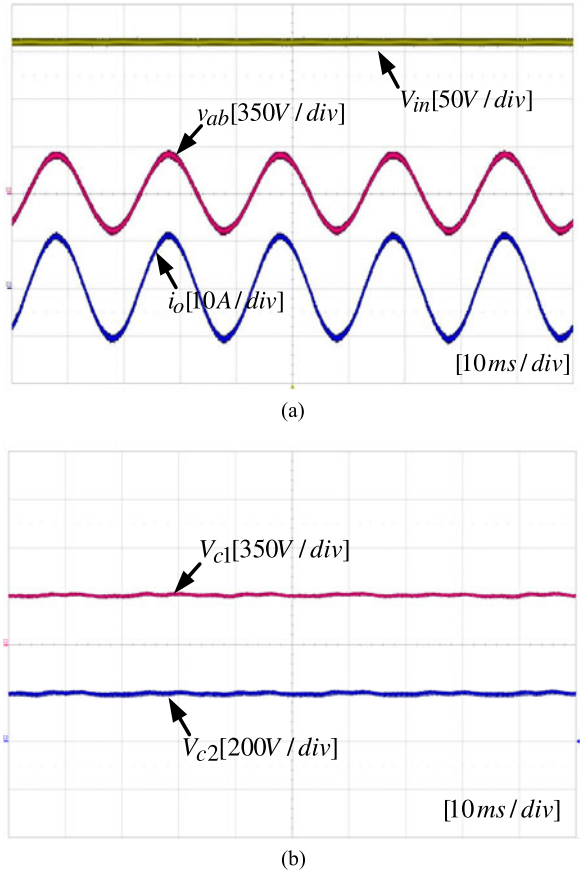

Fig. 18. Experimental waveforms of improved ΓZSI with clamping diode. (a) Input voltage, line-to-line output voltage, and output current. (b) Capacitor voltages.

without D_2 in Fig. 19(b). It clearly shows the added benefit of clamping diode which eliminates the voltage spikes caused by leakage inductances of the transformer. Fig. 20 shows the experimental waveforms of output inductor currents. Fig. 21 shows the picture of improved ΓZSI with clamping diode experimental setup.

VI. Efficiency Calculation

In this section, the efficiencies of improved ΓZSI with clamping diode, conventional ΓZSI, and ΓZSI with *LC* filter are compared. The method used in [7] and [8] for efficiency calculation is adopted here and PSIM simulations are performed considering some loss related parameters, which are listed in Table II.

TABLE II

IGBT (Six Pack)	CM100TU-12H
Diode	STTH60L06C
Core	EE 110/114/36
Capacitor ESR	2.5 mΩ (100 μF)
Copper wire resistivity (ρ)	1.724 μ Ω-cm

The main power losses within an inverter are semiconductor switching and conduction losses, inductor and transformer core losses and its winding resistance, and losses in the equivalent series resistance (ESR) of the capacitors. Among them, the semiconductor losses are the most prominent and biggest. The semiconductor losses are calculated using a thermal module in PSIM simulations. Moreover, as it can be seen from the experiment and simulation results, the improved ΓZSI with clamping diode clearly reduces the voltage overshoots as the leakage inductance energy is recycled through the additional diode without creating voltage spikes, unlike the other inverters in which the leakage inductance energy creates high voltage spikes across the switching devices. Thus, it can use 600-V IGBT

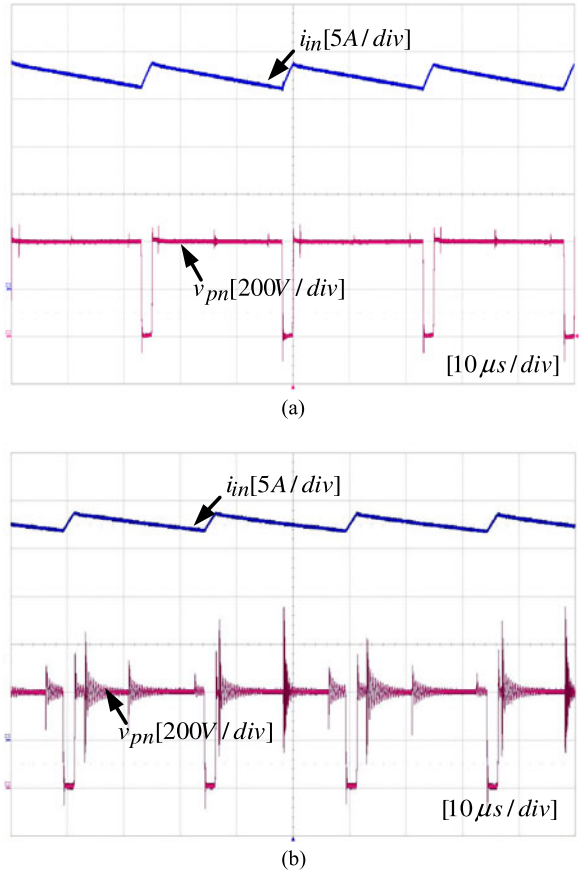

Fig. 19. Experimental waveforms of dc-link voltage and input current. (a) With clamping diode D_2. (b) Without clamping diode D_2.

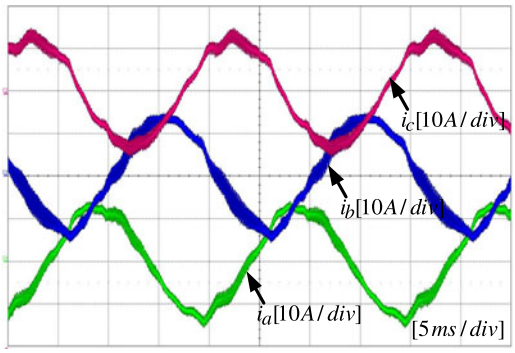

Fig. 20. Experimental waveforms of output inductor currents.

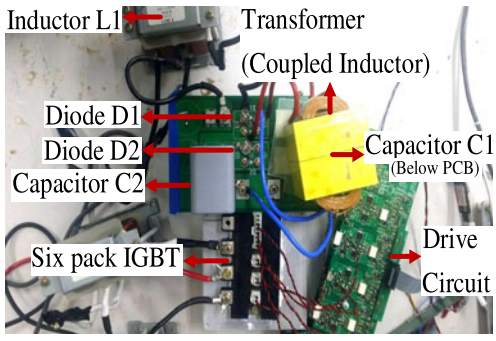

Fig. 21. Hardware prototype of improved ΓZSI with clamping diode.

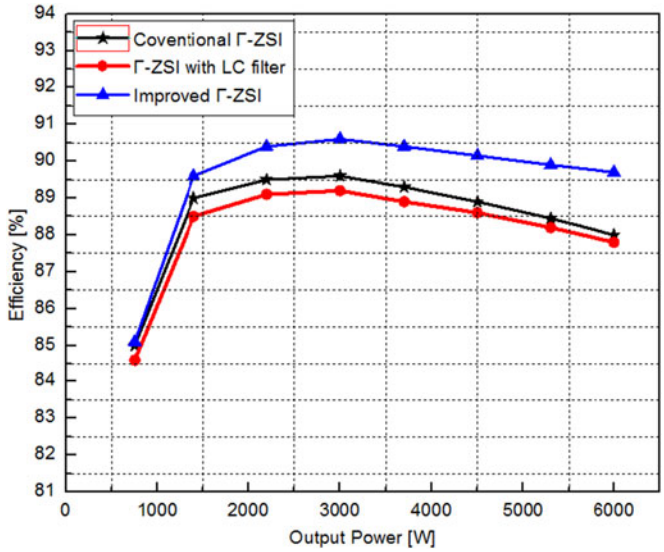

Fig. 22. Efficiency comparison.

module having almost four times smaller switching and conduction losses [33] compared to 1200-V IGBT module, which has to be used for conventional ΓZSI and ΓZSI with *LC* filter. The power losses in the magnetic components consists of its core loss and copper loss, and the equations for calculating the power loss are given in [7] and [34]. The core loss is calculated by

$$P_{fe} = K_{fe}(\Delta B)^{\beta} A_c l_m . \tag{20}$$

The inductor and transformer copper losses can be calculated by

$$\begin{aligned} P_{L\_cu} &= \rho N^2 \mathrm{MLTI}^2 / K_u W_A \\ P_{T\_cu} &= (N_1 I_1 + N_2 I_2)^2 \rho \mathrm{MLT} / K_u W_A \end{aligned} \tag{21}$$

where K_{fe} is the proportionality constant, ΔB is the flux density, β is determined by the core manufacturers sheet, A_c is the cross-sectional area, l_m is the mean core length, ρ is the resistivity, N is the winding turns, I is the rms winding current, (MLT) is the winding mean length per turn, K_u is the winding fill factor, and W_A is the core window area. Additionally, the improved ΓZSI gain is higher than conventional ΓZSI, thus it requires small inductance as compared to conventional ΓZSI, which results in lower winding resistance and losses.

Under these conditions, the efficiencies of the three inverters are plotted and shown in Fig. 22. From the plot, it can be seen that despite having more components than conventional ΓZSI, the improved ΓZSI has higher efficiency because of much smaller switching losses and winding losses due to the utilization of higher modulation index (small shoot-through interval) and clamping diode.

VII. Conclusion

In this paper, an improved ΓZSI with clamping diode was presented in detail. Compared to the conventional ΓZSI topology, the improved inverter inherits the main advantages which are: 1) continuous input current and improved input profile, 2) minimization of the voltage spikes caused by the leakage inductance of the transformer, and 3) higher voltage gain. For the

same input and output voltage conditions, higher modulation index with lower shoot-through duty can be used thus resulting in lower component voltage stresses, better output power quality, and increased efficiency. The improved inverter is best suited for applications that require a single-step high voltage conversion with low-input dc voltage such as fuel cells and PV cells. A 7-kW hardware prototype is constructed and experiments are performed to validate its working operation and benefits.

REFERENCES

[1] M. Shen, A. Joseph, J. Wang, F. Z. Peng, and D. J. Adams, "Comparison of traditional inverters and Z-source inverter for fuel cell vehicles," *IEEE Trans. Power Electron.*, vol. 22, no. 4, pp. 1453–1463, Jul. 2007.

[2] F. Z. Peng, "Z-source inverter," *IEEE Trans. Ind. Appl.*, vol. 39, no. 2, pp. 504–510, Mar./Apr. 2003.

[3] J. Anderson and F. Z. Peng, "Four quasi-Z-source inverters," in *Proc. IEEE Power Electron. Spec. Conf.*, Jun. 2008, pp. 2743–2749.

[4] C. J. Gajanayake, F. L. Luo, H. B. Gooi, and L. K. Siow, "Extended-boost Z-source inverters," *IEEE Trans. Power Electron.*, vol. 25, no. 10, pp. 2642–2652, Oct. 2010.

[5] W. Qian, F. Z. Peng, and H. Cha, "Trans-Z-source inverters," *IEEE Trans. Power Electron.*, vol. 26, no. 12, pp. 3453–3463, Dec. 2011.

[6] M. Adamowicz, R. Strzelecki, F. Z. Peng, J. Guzinski, and H. A. Rub, "New type LCCTZ-Z-source inverters," in *Proc. Eur. Conf. Power Electron.*, 2011, pp. 1–10.

[7] M.-K. Nguyen, Y.-C. Lim, and S.-J. Park, "Improved trans-Z-source inverter with continuous input current and boost inversion capability," *IEEE Trans. Power Electron.*, vol. 28, no. 10, pp. 4500–4600, Oct. 2013.

[8] M. K. Nguyen, Y. C. Lim, and Y. Kim, "TZ-source inverters," *IEEE Trans. Ind. Electron.*, vol. 12, no. 60, pp. 5686–5695, Dec. 2013.

[9] Y. P. Siwakoti, F. Blaabjerg, and P. C. Loh, "New magnetically coupled impedance (Z-) source networks," *IEEE Trans. Power Electron.*, vol. 31, no. 11, pp. 7419–7435, Nov. 2016.

[10] P. C. Loh, D. Li, and F. Blaabjerg, "Γ-Z-source inverters," *IEEE Trans. Power Electron.*, vol. 28, no. 11, pp. 4880–4884, Nov. 2013.

[11] M. R. Banaei, R. Alizadeh, N. Jahanyari, and E. S. Najmi, "An ac Z-source converter based on gamma structure with safe-commutation strategy," *IEEE Trans. Power Electron.*, vol. 31, no. 2, pp. 1255–1262, Feb. 2016.

[12] F. Z. Peng, M. Shen, and Z. Qian, "Maximum boost control of the Z-source inverter," *IEEE Trans. Power Electron.*, vol. 20, no. 4, pp. 833–838, Jul. 2005.

[13] M. Shen *et al.*, "Constant boost control of the Z-source inverter to minimize current ripple and voltage stress," *IEEE Trans. Ind. Appl.*, vol. 42, no. 3, pp. 770–778, May/Jun. 2006.

[14] S. Liu, B. Ge, X. Jiang, H. Abu-Rub, and F. Z. Peng, "Comparative evaluation of three Z-source/quasi-Z-source indirect matrix converters," *IEEE Trans. Ind. Electron.*, vol. 62, no. 2, pp. 692–701, Feb. 2015.

[15] L. He, S. Duan, and F. Z. Peng, "Safe-commutation strategy for the novel family of quasi-Z-source AC/AC converter," *IEEE Trans. Ind. Informat.*, vol. 9, no. 3, pp. 1538–1547, Aug. 2013.

[16] B. Ge, Q. Lei, W. Qian, and F. Z. Peng, "A family of Z-source matrix converters," *IEEE Trans. Ind. Electron.*, vol. 59, no. 1, pp. 35–46, Jan. 2012.

[17] X. P. Fang, Z. M. Qian, and F. Z. Peng, "Single phase Z-source PWM ac-ac converters," *IEEE Power Electron. Lett.*, vol. 3, no. 4, pp. 121–124, Dec. 2005.

[18] D. Vinnikov and I. Roasto, "Quasi-Z-source-based isolated dc/dc converters for distributed power generation," *IEEE Trans. Ind. Electron.*, vol. 58, no. 1, pp. 192–201, Jan. 2011.

[19] Z. Aleem, D. Shin, H. Cha, J. P. Lee, D. W. Yoo, and F. Z. Peng, "Parallel operation of inverter using trans-Z-source network," *IET Power Electron.*, vol. 8, no. 11, pp. 2176–2183, 2015.

[20] Z. J. Zhou, X. Zhang, P. Xu, and W. X. Shen, "Single-phase uninterruptible power supply based on Z-source inverter," *IEEE Trans. Ind. Electron.*, vol. 55, no. 8, pp. 2997–3004, Aug. 2008.

[21] L. Zhang, K. Sun, Y. Xing, L. Feng, and H. Ge, "A modular grid-connected photovoltaic generation system based on dc bus," *IEEE Trans. Power Electron.*, vol. 2, no. 26, pp. 523–531, Feb. 2011.

[22] S. Rajakaruna and L. Jayawickrama, "Steady-state analysis and designing impedance network of Z-source inverters," *IEEE Trans. Ind. Electron.*, vol. 57, no. 7, pp. 2483–2491, Jul. 2010.

[23] C. J. Gajanayake, D. M. Vilathgamuwa, and P. C. Loh, "Development of a comprehensive model and a multiloop controller for Z-source inverter DG systems," *IEEE Trans. Ind. Electron.*, vol. 54, no. 4, pp. 2352–2359, Aug. 2007.

[24] M. Zhu, K. Yu, and F. L. Luo, "Switched inductor Z-source inverter," *IEEE Trans. Power Electron.*, vol. 25, no. 8, pp. 2150–2158, Aug. 2010.

[25] M. Shen and F. Z. Peng, "Operation modes and characteristics of the Z-source inverter with small inductance or low power factor," *IEEE Trans. Ind. Electron.*, vol. 55, no. 1, pp. 89–96, Jan. 2008.

[26] M.-K. Nguyen, Y.-C. Lim, and G.-B. Cho, "Switched-inductor quasi-Z-source inverter," *IEEE Trans. Power Electron.*, vol. 26, no. 11, pp. 3183–3191, Nov. 2011.

[27] Q. Tran, T. Chun, J. Ahn, and H. Lee, "Algorithms for controlling both the DC boost and AC output voltage of Z-source inverter," *IEEE Trans. Ind. Electron.*, vol. 54, no. 5, pp. 2745–2750, Oct. 2007.

[28] B. Zhao, Q. Yu, Z. Leng, and X. Chen, "Switched Z-source isolated bidirectional dc-dc converter and its phase-shifting shoot-through bivariate coordinated control strategy," *IEEE Trans. Ind. Electron.*, vol. 59, no. 12, pp. 4657–4670, Dec. 2012.

[29] Z. Aleem, H. F. Ahmed, H. Cha, and H.-G. Kim, "Single-phase isolated impedance-source inverters," in *Proc. Int. Conf. Power Electron.*, Jun. 2015, pp. 2359–2364.

[30] D. Xinping and Z. Chenghui, "Switched coupled-inductor Z-source inverters with large conversion ratio and soft-switching condition," in *Proc. IEEE Energy Convers. Congr. Expo.*, 2014, pp. 5052–5058.

[31] H. Cha, Y. Li, and F. Z. Peng, "Practical layouts and DC-rail voltage clamping techniques of Z-source inverters," *IEEE Trans. Power Electron.*, vol. 31, no. 11, pp. 7471–7479, Nov. 2016.

[32] W. Mo, P. C. Loh, and F. Blaabjerg, "Asymmetrical Γ-source inverters," *IEEE Trans. Ind. Electron.*, vol. 61, no. 2, pp. 637–647, Feb. 2014.

[33] P. J. Grbovic, P. Delaure, and P. L. Moigne, "A novel three-phase diode boost rectifier using hybrid half-dc-bus-voltage rated boost converter," *IEEE Trans. Ind. Electron.*, vol. 58, no. 4, pp. 1316–1329, Apr. 2011.

[34] R. W. Erickson and D. Maksimovic, *Fundamentals of Power Electronics*. Norwell, MA, USA: Kluwer, ch. 15, 2001.

Zeeshan Aleem (S'15) received the B.S. degree in computer engineering from Comsats Institute of Information Technology, Islamabad, Pakistan in 2013, and the M.S. degree in energy engineering from Kyungpook National University, Daegu, South Korea, in 2015.

In 2015, he joined the Power Electronics Research Group as a Postgraduate Researcher in the Department of Electrical Engineering, University of Cape Town, Cape Town, South Africa. His current research interests include high-frequency magnetics, high-power dc–dc converters, impedance-source inverters, *Z*-source ac–ac converters, and grid-connected inverters.

Moin Hanif (M'11) received the B.Eng. (Hons.) degree (first class) in electrical and electronic engineering from the University of Nottingham, Nottingham, U.K., in 2007, and the Ph.D. degree in power electronics from Dublin Institute of Technology (DIT), Dublin, Ireland, in 2011.

He was a Postdoctoral Researcher at Masdar Institute of Science and Technology, United Arab Emirates, from October 2011 to 2012. From November 2012 to December 2016, he was a Senior Lecturer in the Department of Electrical Engineering, University of Cape Town (UCT), Cape Town, South Africa. Since January 2016, he has been full-time Faculty at DIT, and concurrently since March 2017, he has also been a Visiting Academic at the University of Johannesburg, Johannesburg, South Africa. His current research interests include power electronics converters and their control, MPPT of PV power, islanding detection, grid integration of renewables, micro/smart grid operation, and wireless power transfer.

Dr. Hanif has received a number of research grants from the UCT and the Government of South Africa and also serves as a Program Committee Member for IEEE conferences.